

Evaluation of Different Front Surface Passivation Schemes for p-type IBC Solar Cells

Marius Meßmer^{1,*} , Lazhar Rachdi² , Pierre Saint-Cast¹, Stefan Schmidt¹, Nico Jung¹, Jan Lossen² , and Andreas Wolf¹

¹Fraunhofer Institute for Solar Energy Systems (ISE), Germany

²International Solar Energy Research Center (ISC) Konstanz, Germany

*Correspondence: Marius Meßmer, marius.messmer@ise.fraunhofer.de

Abstract. In this work, we investigate different front-side passivation approaches for p-type IBC solar cells. We compare a POCl₃-diffused and SiN_x-passivated front floating emitter (FFE) with an undiffused front surface passivated by a layer stack of aluminum oxide Al₂O₃ and silicon nitride SiN_x, using different technologies for Al₂O₃ deposition. Further, we investigate a boron-doped front surface field (FSF), realized with different BBr₃ diffusion approaches. We achieve promising implied open-circuit voltages iV_{oc} of up to 740 mV with Al₂O₃/SiN_x-passivation, which is a 7 mV increase compared to the reference process using the phosphorus-doped FFE. Further, we fabricated boron-doped FSF samples exhibiting promising recombination parameters of $j_0 < 6$ fA/cm². The transfer of the Al₂O₃/SiN_x-passivation into pIBC solar cells already reaches peak efficiencies of $\eta = 23.3\%$, comparable to the FFE.

Keywords: pIBC, PE-ALD, ALD, FSF, Passivation

1. Introduction

In the last years, photovoltaic industry is switching from the fabrication of passivated emitter and rear (PERC) solar cells [1] towards tunnel oxide passivating contact (TOPCon) solar cells [2], due to higher efficiency potential. Nevertheless, many PERC lines are available in industry, which could be easily upgraded to an interdigitated back contact (IBC) solar cell line for p-type wafers by adding a tool for the poly-Si deposition and a laser for structuring [3, 4]. The IBC structure, which has been investigated by many others with different approaches, e.g. [5-10], offers a cost-effective solar cell structure with high efficiency potential. Further, IBC offers reduced silver consumption, due to the use of aluminum as a p-contact. Reducing silver consumption in TOPCon fabrication is crucial for a sustainable terawatt scale PV production [11]. Our pIBC solar cell features a carrier-selective n-poly-Si contact which enables an efficiency potential of >25% [12]. Currently, a phosphorus oxychloride (POCl₃) diffusion process forms a front floating emitter (FFE), simultaneously crystallizes the poly-Si layer and forms a PSG layer that serves as an etch barrier in the wet-chemical etching step for rear side structuring [4]. Nevertheless, this FFE limits the efficiency due to front side recombination ($j_{0,FFE} > 10$ fA/cm²). Therefore, we investigate two alternative front side architectures: An undiffused surface passivation with Al₂O₃/SiN_x passivation layers and a boron-doped front surface field formed by a thermal boron diffusion process passivated with Al₂O₃/SiN_x. These approaches are also applicable on other IBC structures.

2. Experimental

2.1 Test structures

2.1.1 Development of $\text{Al}_2\text{O}_3/\text{SiN}_x$ passivation on p-type silicon

In back contact solar cells, the passivation of the front-side is an important factor. Due to the generation of the charge carriers on this side of the solar cell, the minority carriers need to diffuse through the whole bulk until they reach the emitter region on the rear side. In this investigation, the front side passivation of the textured and undiffused p-type surface of the pIBC solar cell, by a layer stack of aluminum oxide Al_2O_3 and silicon nitride SiN_x is developed. Figure 1 shows the applied process flow for the development. We used Czochralski-grown gallium-doped silicon wafers (Cz-Si:Ga) with a base resistivity ρ_b of $\rho_b = 5$ to $7 \Omega\text{cm}$ in M2 (156.75 x 156.75 mm) format. First, the surface is textured with random pyramids in an alkaline solution, followed by a wet-chemical cleaning step. Subsequently, a variation of a batch atomic layer deposition (ALD) process is performed. The varied important parameters of the batch ALD process are the temperature T_{ALD} and the number of cycles cy_{ALD} , which is proportional to the grown Al_2O_3 layer thickness. We varied the ALD parameter with 4 different temperatures T_{ALD} in 20K steps as well as 5 different numbers of cycles in steps of 10 cycle each. After the ALD process, half of the samples went through a thermal annealing process to prevent layer blistering. Now, both-sided silicon nitride SiN_x layers are deposited as an anti-reflection layer by means of plasma-enhanced chemical vapor deposition (PECVD). As a final process step, all samples undergo a firing process in an infrared firing furnace at a set temperature of $T_{\text{set}} = 800^\circ\text{C}$ to mimic the cell fabrication process. Finally, the effective carrier lifetime of the samples is characterized by quasi-steady state photoconductance (QSSPC) measurement.

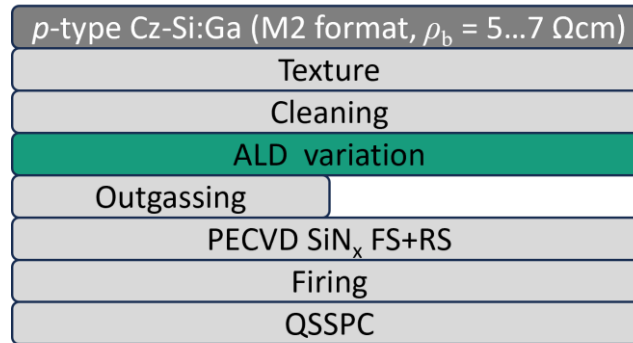


Figure 1. The process flow for the development of $\text{Al}_2\text{O}_3/\text{SiN}_x$ layer stack passivation on textured p-type silicon surface is depicted

2.1.2 Development of boron front-surface field passivation

As an alternative front-side we investigated a boron-diffused front surface field (FSF) with $\text{Al}_2\text{O}_3/\text{SiN}_x$ passivation, using the process flow depicted in Figure 2. On the left half, textured wafers are used, whereas the right half uses saw-damage etched (SDE) wafers. Both types of surfaces are wet-chemical cleaned prior to the boron diffusion using boron tribromide BBr_3 as liquid dopant precursor in a tube furnace. We compared two types of boron processes. The first process, depicted as "BBr₃ diffusion" is similar to a conventional boron diffusion process, containing a deposition phase with active BBr_3 flux and a subsequent drive-in step including in-situ oxidation [13]. The second boron process is reduced to the deposition phase where the borosilicate glass (BSG) layer grows on the wafer surface. This process, denoted as "BBr₃ deposition", omits further drive-in and in-situ oxidation steps. For the textured samples, a thermal tunnel-oxide process is performed as in the solar cell process flow. Furthermore, all samples receive wet chemical cleaning prior to the thermal annealing process. This annealing process, which crystallizes the poly-Si layer in the solar cell process flow, simultaneously serves

as a dopant drive-in for the samples with the "BBr₃ deposition" process. Prior to the BSG etching for all the samples, the emitter sheet resistance R_{sh} of the SDE samples is characterized by four-point probe and inductive R_{sh} measurement. Electrochemical capacitance voltage (ECV) [14] measurement yields the doping profile on the SDE samples. A stack of ALD Al₂O₃ and PECVD SiN_x passivates the textured samples on both sides. After the firing process, QSSPC measurements and the evaluation procedure by *Kimmerle et al.* [15] yields the recombination parameter j_0 .

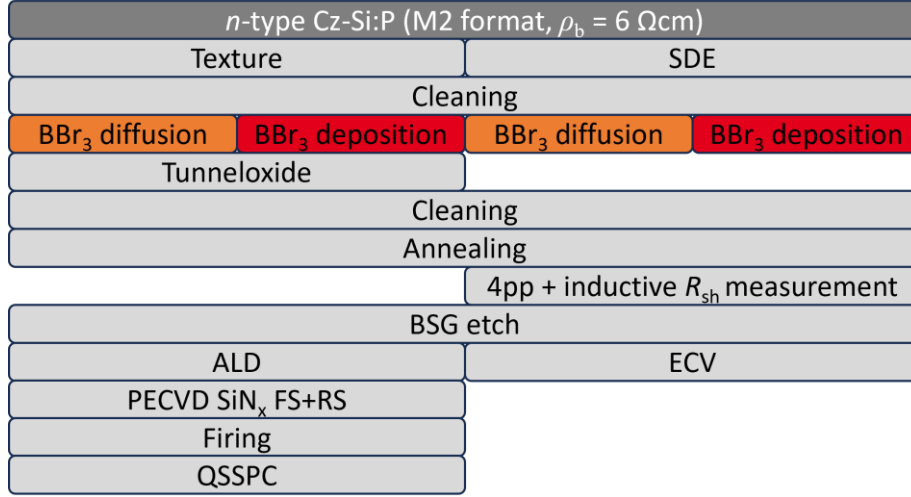


Figure 2. Process flow for the characterization of the boron-diffused FSF characteristics like recombination parameter j_0 , sheet resistance R_{sh} and doping profile

2.2 Solar cells

In this work, different front side passivation schemes are integrated into the pIBC solar cell process. The fabrication process flow is depicted in Figure 3. Group G1 features the FFE [4] and represents the reference process. Groups G2 and G3 investigate the passivation of the undoped *p*-type front surface with an Al₂O₃/SiN_x layer stack. Group G4 uses a boron FSF with Al₂O₃/SiN_x-passivation. All groups use *p*-type Cz-Si:Ga wafers with $\rho_b = 1.8 \Omega\text{cm}$ in M2 format, which are alkaline textured. For groups G1 to G3, a PECVD silicon oxide SiO_x layer serves as a single front-side barrier for the subsequent etching of the rear side in an alkaline potassium hydroxide (KOH) solution. After removal of the rear side texturing, the SiO_x etching barrier is removed in hydrofluoric acid (HF). For group G4 a boron diffusion process (maximum temperature $T_{max} > 1000^\circ\text{C}$) is performed, where the BSG layer acts as an etching barrier. Prior to the chemical etch isolation (CEI), the BSG layer is removed on the rear side of the wafer. Subsequently, the rear side emitter is removed, and the surface is polished during the CEI process. A cleaning step is performed prior to the thermal oxidation process to form the tunnel oxide layer underneath the n-doped poly-Si layer which is then deposited on the rear side using a PECVD tool. For group G1, a phosphorus oxychloride (POCl₃) diffusion process serves as poly-Si crystallization process and simultaneously forms the FFE on the front side. For groups G2-G4 an anneal process crystallizes the poly-Si layer. In the following laser structuring process, the poly-Si layer is ablated on the rear side. Now, chemical etching in an alkaline solution removes the laser damage in the opened areas. After wet-chemical cleaning, the reference group G1 is passivated by a stack of a thin thermal oxide and PECVD SiN_x layer on the front side and a PECVD AlO_x/SiN_x stack on the rear side. Group G2 includes a thermal atomic layer deposited (ALD) aluminum oxide (Al₂O₃) layer on both sides and an outgasing step to remove excess hydrogen from the Al₂O₃ layer. The front and rear side of the group G2 samples are coated with an PECVD SiN_x layer, here specific recipes for capping of ALD layers were applied. Group G3 and G4 uses PE-ALD Al₂O₃ and PECVD SiN_x layers on front and rear side. After the deposition of the passivation layers, some samples are extracted and fired to determine the implied open-circuit voltage iV_{oc} by QSSPC measurement. The remaining samples are

further fabricated to pIBC solar cells. On the rear side, a laser contact opening (LCO) process ablates the passivation layers in the earlier ablated areas for the p-contact formation. The metallization is performed using screen-printing of silver pastes on the poly-Si areas (n-contact) and aluminum paste on the LCO for the p-contact, followed by a contact firing process which forms the metal contacts. Finally, the current voltage (*IV*) characteristics of the solar cells are measured. A regeneration process in a firing furnace is then performed prior to a further *IV* measurement.

G1: FFE (reference)	G2: undiffused A	G3: undiffused B	G4: Boron-FSF
p-type Cz-Si:Ga (M2 format, $\rho_b = 1.8 \Omega\text{cm}$)			
Texture			
PECVD FS SiO _x			BBr ₃ process
RS KOH etching			RS BSG etching
FS SiO _x etching + cleaning			CEI + cleaning
Thermal oxidation			
RS PECVD Poly-Si (n)			
POCl ₃ FFE	Poly-Si annealing		
Laser structuring			
Chemical etching / Cleaning			
Thermal oxidation	ALD Al ₂ O ₃ both sides	FS PE-ALD Al ₂ O ₃ + FS PECVD SiN _x	
	Outgassing		
FS PECVD SiN _x		RS PE-ALD Al ₂ O ₃ + RS PECVD SiN _x	
RS PECVD AlO _x +SiN _x	RS PECVD SiN _x		
Laser contact opening LCO			
Silver screen printing			
Aluminum screen printing			
Contact firing			
IV measurement			
Regeneration process			
IV measurement			

Figure 3. Process flow for the fabrication of *p*-type IBC solar cells with different front side passivation schemes

3. Results and Discussion

3.1 Test structures

3.1.1 Development of Al₂O₃/SiN_x passivation on *p*-type silicon

For the front side passivation scheme using ALD Al₂O₃ and PECVD SiN_x on the undiffused *p*-type wafer, we optimized our batch ALD process, as described in section 2.1.1. Figure 4 shows the average values and standard deviation of the effective carrier lifetimes τ determined by QSSPC on 3 samples with 5 positions over the wafer at an injection level of $\Delta n = 1 \cdot 10^{15} \text{ cm}^{-3}$. For most of the investigated process combinations without an outgassing process, we did not observe any blistering. Nevertheless, for all process combinations, except the highest T_{ALD} and cy_{ALD} , outgassing is beneficial for the resulting lifetime. Starting from a carrier lifetime τ of $\tau = (431 \pm 56) \mu\text{s}$ for very thin layers deposited at the lowest T_{ALD} , increasing cy_{ALD} increases τ for the same T_{ALD} . This holds for all investigated T_{ALD} except the highest T_{ALD} and shows room for improvement with even thicker layers at higher cy_{ALD} . At the highest investigated T_{ALD} , τ first increases from $\tau = (1189 \pm 113) \mu\text{s}$ to $\tau = (1512 \pm 240) \mu\text{s}$ when increasing cy_{ALD} , which is the highest lifetime in this investigation. Further increasing cy_{ALD} decreases the lifetime again to $\tau = (822 \pm 185) \mu\text{s}$.



Lifetime / μs		ALD temperature $T_{\text{ALD}} / ^\circ\text{C}$				Outgas	
		Low				High	yes/no
Number of ALD cycles cy_{ALD}		Low	461 ± 56				yes
			125 ± 16				no
			611 ± 48	626 ± 36	925 ± 76		yes
			564 ± 34	567 ± 39	822 ± 51		no
				1297 ± 105	1227 ± 185	1189 ± 113	yes
				1227 ± 28	992 ± 75	738 ± 85	no
					1354 ± 142	1512 ± 240	yes
					957 ± 61	848 ± 41	no
						822 ± 185	yes
						1034 ± 169	no

Figure 4. Average value and standard deviation of the effective carrier lifetime determined by QSSPC at $\Delta n = 1 \cdot 10^{15} \text{ cm}^{-3}$ for samples with ALD Al_2O_3 -passivated, textured p-type surface using different temperatures and number of cycles. The samples are capped with SiN_x and fired

3.1.2 Development of boron front-surface field passivation

For the alternative front side using a boron-doped front surface field (FSF), two different BBr_3 tube furnace processes are investigated as described in section 2.1.2. Figure 5 a) shows the doping profiles measured on n-type wafers by ECV. Already during the BBr_3 deposition process, boron diffuses into the silicon wafer and forms a doping profile with a maximum charge carrier concentration N_{max} of $N_{\text{max}} = 1.6 \cdot 10^{19} \text{ cm}^{-3}$ and a junction depth X of $X \approx 180 \text{ nm}$ at a concentration of $N = 1 \cdot 10^{18} \text{ cm}^{-3}$.

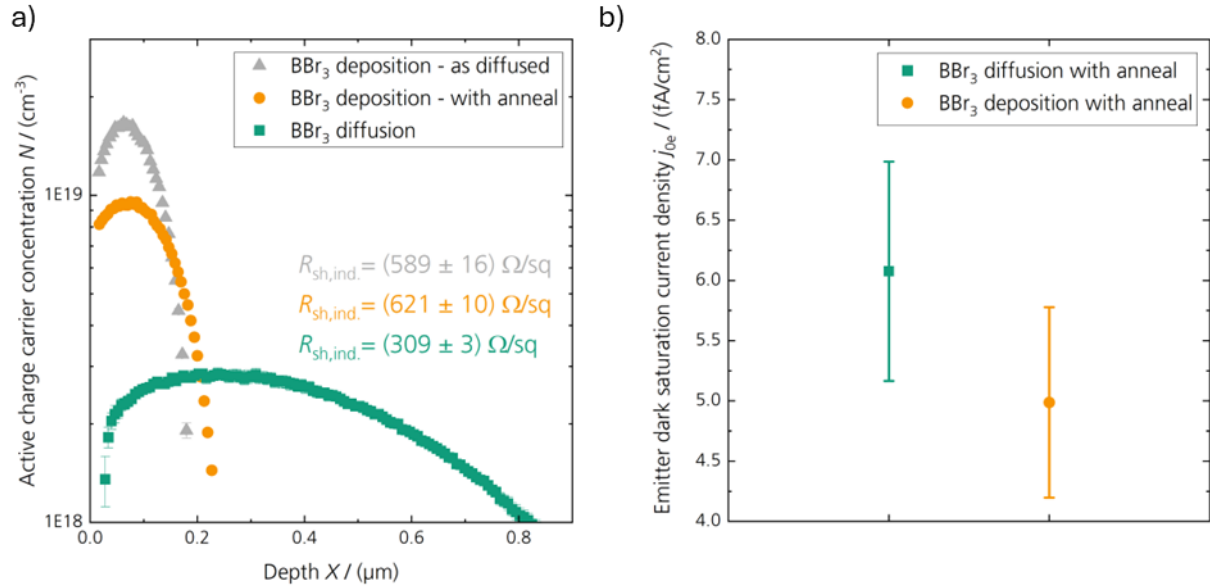


Figure 5. a) Doping profiles for the BBr_3 deposition without and with anneal as well as the conventional BBr_3 diffusion process measured by ECV. Inductive sheet resistance measurement results are further stated in the graph for the respective process. b) Recombination parameter j_0 for the BBr_3 processes

The inductive sheet resistance measurement yields $R_{\text{sh}} = (589 \pm 16) \Omega/\text{sq}$ for this profile. During the poly-Si annealing process for the pIBC solar cell, with un-etched BSG, the doping profile changes as well. The boron atoms redistribute inside of the silicon. The maximum concentration reduces to $N_{\text{max}} = 9.5 \cdot 10^{18} \text{ cm}^{-3}$ while the junction depth increases to $X \approx 230 \text{ nm}$.

The emitter sheet resistance increases slightly to $R_{sh} = (621 \pm 10) \Omega/\text{sq}$. The conventional boron diffusion process includes a high temperature drive-in and results in an emitter sheet resistance of $R_{sh} = (309 \pm 3) \Omega/\text{sq}$ with a much lower maximum concentration of $N_{\text{max}} = 2.8 \cdot 10^{18} \text{ cm}^{-3}$ and a significantly higher depth with $X \approx 800 \text{ nm}$ compared to the BBr_3 deposition approach. We determine the recombination parameter j_0 by QSSPC measurements on symmetrical carrier lifetime samples, as described in section 2.1.2, shown in Figure 5 b). Using the slope method from *Kimmerle et al.* [15] for the evaluation yields promising $j_{0e} = (6.1 \pm 0.9) \text{ fA/cm}^2$ for the BBr_3 diffusion approach and even lower $j_{0e} = (5.0 \pm 0.8) \text{ fA/cm}^2$ for the BBr_3 deposition with anneal approach. The latter represents a lean process flow with low thermal budget.

3.2 Solar cells

With the process flow described in section 2.2, unmetallized solar cell precursors are fabricated and characterized by QSSPC. Figure 6 a) shows the unmetallized solar cell precursor with the different front-side schemes. On the left, the doped front-side with phosphorus and boron doping is schematically depicted. On the right, the undiffused structure with $\text{Al}_2\text{O}_3/\text{SiN}_x$ passivation is shown. Figure 6 b) shows the asymmetrical base region, representing the p-contact region in the solar cell. Figure 6 c) shows the implied open-circuit voltage iV_{oc} , the voltage potential of the solar cell. The reference scheme with the POCl_3 FFE reaches $iV_{oc} = (727 \pm 4) \text{ mV}$. Omitting the FFE and passivating the front side with ALD Al_2O_3 and PECVD SiN_x on top (Undiff. A), increases the iV_{oc} by 3 mV to $iV_{oc} = (730 \pm 4) \text{ mV}$. Using a PE-ALD Al_2O_3 process (Undiff. B) further increases the iV_{oc} to promising $iV_{oc} = (734 \pm 5) \text{ mV}$ with a peak at 740 mV. Using a boron FSF reaches only $iV_{oc} = (710 \pm 7) \text{ mV}$, despite the promising j_{0e} results shown in the previous section 3.1.2. The measurements in the base regions show $iV_{oc} = (715 \pm 9) \text{ mV}$ for "Undiff. A" and $iV_{oc} = (724 \pm 9) \text{ mV}$ for "Undiff. B" and $iV_{oc} = (693 \pm 6) \text{ mV}$ for the boron FSF. These measurements show that currently this region limits the potential of our pIBC structure.

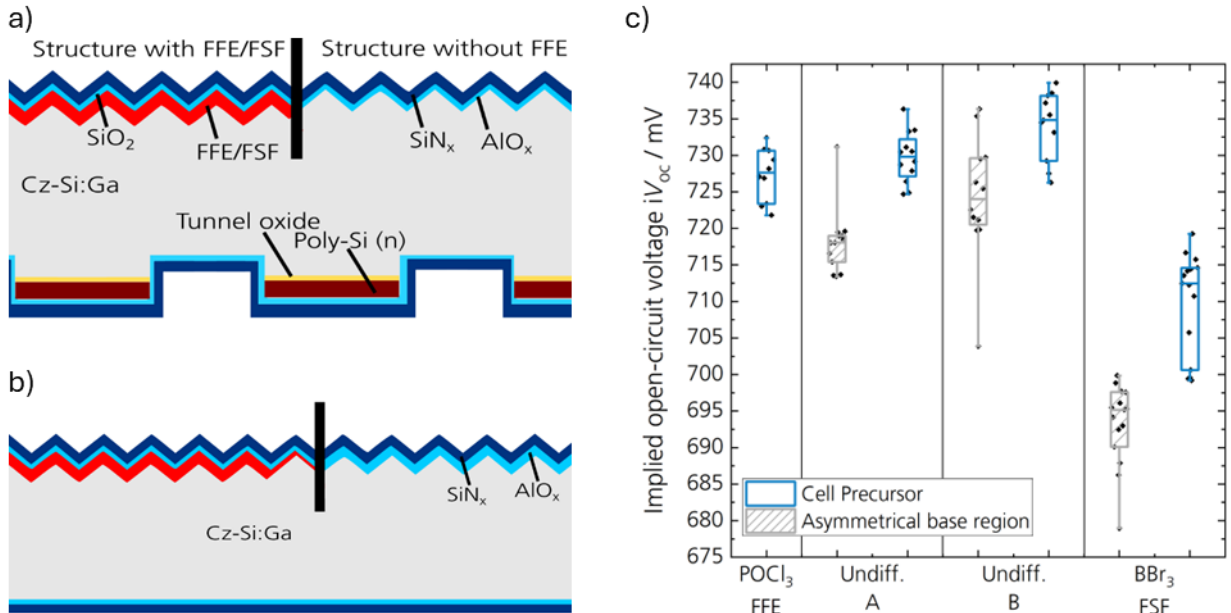


Figure 6. a) Schematic structure of unmetallized cell precursors with different front sides. b) Schematic structure of the unmetallized base region. c) Voltage potential of the pIBC solar cells measured on unmetallized structures by QSSPC

Figure 7 shows the IV characteristics before and after a regeneration process for the fabricated pIBC solar cells. In general, the regeneration process mainly increases the open-circuit voltage V_{oc} and the pseudo fill factor pFF of the solar cells for all groups. The reference POCl_3

FFE reaches an energy conversion efficiency of $\eta = (22.8 \pm 0.3)\%$ with a maximum of $\eta = 23.3\%$. Omitting the FFE and passivating the front-side with both-sided ALD Al_2O_3 and PECVD SiN_x with non-optimized ALD layer results in similar V_{oc} of $V_{oc} = (710 \pm 2)$ mV compared to the reference FFE, but results in a reduced short-circuit current density j_{sc} of $j_{sc} = (40.1 \pm 0.2)$ mA/cm² which is 0.6 mA/cm² lower than the reference FFE. Improving the SiN_x layer as the anti-reflection coating might improve the j_{sc} . Switching to PE-ALD Al_2O_3 for the undiffused surface results in an increased V_{oc} by 7 mV to $V_{oc} = (717 \pm 3)$ mV but still reduced j_{sc} which is 0.4 mA/cm² lower than the reference FFE. Overall, this approach reaches similar energy conversion efficiency with $\eta = (22.8 \pm 0.4)\%$ with a similar maximum of $\eta = 23.3\%$. Despite the promising j_{0e} results (see section 3.1.2) the boron FSF results in $\eta = (21.5 \pm 0.3)\%$ due to strongly reduced V_{oc} and j_{sc} . We suggest that the bulk lifetime is affected by the boron diffusion, which leads to low V_{oc} , which needs to be investigated in more detail. Further, the width of the IV parameter indicates that the POCl_3 FFE has the narrowest distribution compared to the undiffused front side. Undiffused front sides are more sensitive against contamination, particles and scratches due to handling. Nevertheless, this aspect of (p)IBC fabrication needs more statistical analysis due to the low amount of solar cells in this investigation.

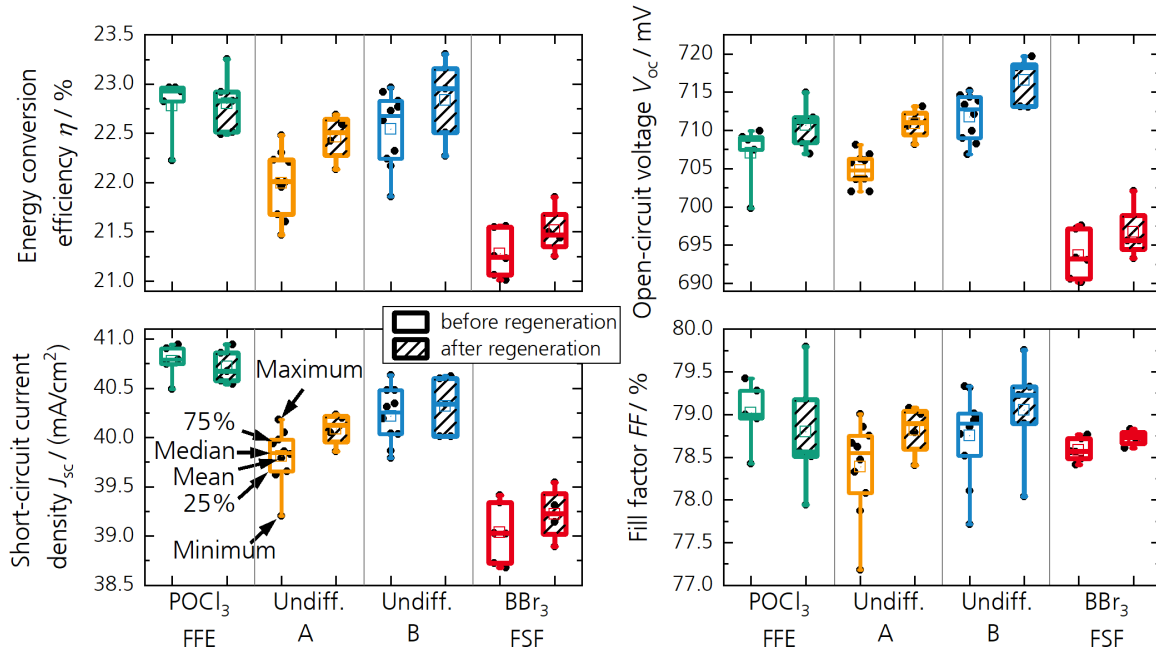


Figure 7. Current-voltage IV characteristics of the pIBC solar cells with different front-side passivation schemes measured by a cell tester after firing as well as after an additional regeneration process in a firing furnace

4. Conclusion

In this work, we investigated different front-side passivation schemes for p-type IBC solar cells: POCl_3 -diffused FFE, different Al_2O_3 / SiN_x passivation and a boron-doped FSF. For this, we improved our ALD Al_2O_3 process and increased the lifetime up to $\tau = (1512 \pm 240)$ μs for symmetric textured p-type samples. For the boron FSF we reached promising emitter recombination parameters lower than $j_{0e} < 6$ fA/cm² with a conventional boron diffusion as well as for a two-stage doping profile formation. Fabricating pIBC solar cells with those front-side passivation schemes results in a peak energy conversion efficiency of $\eta = 23.3\%$ for the POCl_3 FFE reference group as well as for the PE-ALD Al_2O_3 / PECVD SiN_x passivation. Further work will explore the potential of ALD Al_2O_3 on solar cell level as well as the promising j_{0e} for the boron FSF.

Data availability statement

The data that support the findings of this study are available from the corresponding author upon reasonable request.

Author contributions

M. Meßmer: Conceptualization, investigation, visualization, writing – original draft

L. Rachdi: Conceptualization; investigation, review

P. Saint-Cast: Methodology, investigation, review

A. Wolf: Supervision, funding acquisition, review

S. Schmidt: Investigation, review

N. Jung: Investigation, review

J. Lossen: Funding acquisition, review

Funding

The authors would like to acknowledge financial support by the German Federal Ministry of Economic Affairs and Climate Action within the research projects “OLIVIA” (contract number 03EE1184B).

References

- [1] A. W. Blakers, A. Wang, A. M. Milne, J. Zhao, and M. A. Green, “22.8% efficient silicon solar cell,” *Appl. Phys. Lett.*, vol. 55, no. 13, pp. 1363–1365, 1989.
- [2] F. Feldmann, M. Bivour, C. Reichel, M. Hermle, and S. W. Glunz, “Passivated rear contacts for high-efficiency n-type Si solar cells providing high interface passivation quality and excellent transport characteristics,” *Solar Energy Materials and Solar Cells*, vol. 120, pp. 270–274, 2014.
- [3] L. J. Koduvelikulathu, J. Lossen, Adrian A., D. Rudolph, R. Roescu, A. Wolf, B. Steinhäuser, M. Frettlöh, S. Schmidt, T. Pernau, H. Haverkamp, and R. Kopecek, “Industrial feasible screen printed IBC solar cell based on PECVD a-Si (n) deposition on large area p-type substrates,” in *8th World Conference on Photovoltaic Energy Conversion*, 2022.
- [4] L. Rachdi, J. Lossen, D. Rudolph, Y. P. Sharma, L. J. Koduvelikulathu, J.-I. Polzin, S. Schmidt, A. Wolf, and T. Pernau, “Development and Process Optimization of a p-IBC Solar Cell with PECVD Deposited Passivated Contacts,” (en), *40th European Photovoltaic Solar Energy Conference and Exhibition*, 2023.
- [5] A. Mewe, P. Spinelli, A. Burgers, G. Janssen, N. Guillemin, B. van de Loo, E. Kessels, A. Ylooswijk, B. Geerligs, and I. Cesar, “Mercury: Industrial IBC cell with front floating emitter for 20.9% and higher efficiency,” in *2015 IEEE 42nd Photovoltaic Specialist Conference (PVSC)*, New Orleans, LA, 2015, pp. 1–6.
- [6] R. Peibst, F. Haase, B. Min, C. Hollemann, T. Brendemühl, K. Bothe, and R. Brendel, “On the chances and challenges of combining electron-collecting n POLO and hole-collecting Al- p+ contacts in highly efficient p -type c-Si solar cells,” *Prog. Photovolt: Res. Appl.*, vol. 31, no. 4, pp. 327–340, 2023.
- [7] Xiajie Meng, p-type TBC cell and module pilot running in Tongwei. [Online] Available: https://www.backcontact-workshop.com/pdf/2023/8_Tongwei-Solar.pdf. Accessed on: Jul. 16 2025.

- [8] AIKO, ABC solar cell - towards single junction efficiency limit. [Online] Available: https://www.backcontact-workshop.com/pdf/2023/7_Aiko.pdf. Accessed on: Jul. 16 2025.
- [9] David Smith, IBC solar cells: The next technology Node. [Online] Available: https://www.backcontact-workshop.com/pdf/2024/6_Maxeon.pdf. Accessed on: Jul. 16 2025.
- [10] Peijun Shen, HPBC - The best practives for module technologies. [Online] Available: https://www.backcontact-workshop.com/pdf/2022-2/10_Longi.pdf. Accessed on: Jul. 16 2025.
- [11] Y. Zhang, S. Wang, L. Wang, Z. Sun, Y.-C. Chang, R. Chen, C. Chan, K. Okamoto, Y. Ao, D. Wang, M. Dhamrin, T. Kosuke, and B. Hallam, "Ultra-Lean Silver Screen-Printing for Sustainable Terawatt-Scale Photovoltaic," *Sol. RRL*, vol. 8, no. 17, 2024.
- [12] C. N. Kruse, S. Schäfer, F. Haase, V. Mertens, H. Schulte-Huxel, B. Lim, B. Min, T. Dullweber, R. Peibst, and R. Brendel, "Simulation-based roadmap for the integration of poly-silicon on oxide contacts into screen-printed crystalline silicon solar cells," (eng), *Scientific reports*, vol. 11, no. 1, p. 996, 2021.
- [13] S. Werner, E. Lohmüller, U. Belledin, A. Vlooswijk, R. Naber, S. Mack, and A. Wolf, "Optimization of BBr₃ Diffusion Processes for N-type Silicon Solar Cells," in *31st EU PVSEC*, Hamburg, Germany, 2015.
- [14] P. Blood, "Capacitance-voltage profiling and the characterisation of III-V semiconductors using electrolyte barriers," *Semicond. Sci. Technol.*, vol. 1, no. 1, pp. 7–27, 1986.
- [15] A. Kimmerle, J. Greulich, and A. Wolf, "Carrier-diffusion corrected J₀-analysis of charge carrier lifetime measurements for increased consistency," *Solar Energy Materials and Solar Cells*, vol. 142, pp. 116–122, 2015.